



This is the accepted manuscript made available via CHORUS. The article has been published as:

Investigation of octupole deformed fragments decaying
from even-even isotopes of ${}^{222}\text{Th}$ – ${}^{230}\text{Th}$

Shivani Jain, Raj Kumar, S. K. Patra, and Manoj K. Sharma

Phys. Rev. C **105**, 034605 — Published 7 March 2022

DOI: [10.1103/PhysRevC.105.034605](https://doi.org/10.1103/PhysRevC.105.034605)

Investigation of octupole deformed fragments decaying from even-even isotopes of $^{222-230}\text{Th}^*$

Shivani Jain^{1,*}, Raj Kumar¹, S. K. Patra^{2,3}, and Manoj K. Sharma¹

¹*School of Physics and Materials Science, Thapar Institute of Engineering & Technology, Patiala - 147004, Punjab, India*

²*Institute of Physics, Bhubaneswar 751005, India and*

³*Homi Bhabha National Institute, Training School Complex, Anushakti Nagar, Mumbai 400085, India*

Background: In earlier studies, the spherical and quadrupole deformed nuclei with closed shells were found as the most probable fission fragments in the decay of heavy mass compound nuclei at the low excitation energies. Recently, the disintegration of heavy-mass actinides gave the evidence of pear-shaped fission fragments, in the mass-asymmetric region, due to extra stability provided by the shell-stabilized octupole deformed ^{144}Ba ($Z=56$) nucleus.

Purpose: In our theoretical work, we have done an exercise to analyze the possibility of octupole deformed fragments in the decay of light- and heavy-mass isotopes of Thorium, i.e. $^{222,224,226,228,230}\text{Th}^*$.

Method: To carry forward the above idea, the mass- and charge-dispersion of chosen Th isotopes have been analyzed by including deformations (up to β_3) and related cold optimum orientations within the Dynamical Cluster-decay Model (DCM), which is based on the collective clusterization approach of Quantum Mechanical Fragmentation Theory. The above analysis is worked out at the low excitation energy, which corresponds to the cold synthesis criteria.

Results: In the decay of considered Th isotopes, the minima of fragmentation potential and peaks of preformation probability appear in two regions, near-symmetric and asymmetric, respectively due to the presence of quadrupole (β_2) and octupole deformations (β_3) of decay fragments. However, the emission of β_3 -deformed fission fragments is prominent in the heavier isotopes of Th, i.e. $^{226,228,230}\text{Th}^*$. The above result is in agreement with the experimentally obtained mass- and charge-distributions.

Conclusions: The disintegration of Thorium isotopes into octupole deformed fragments in the asymmetric region signifies their relative stability, which is enhanced for ^{144}Ba ($Z = 56$) or in its vicinity.

PACS numbers:

I. INTRODUCTION

A comprehensive knowledge is required to understand the complex behavior of the nuclear fragments emitted in variety of decay channels. Such decaying fragments behave as a source of production of new isotopes/elements away from the beta-stability line, which in turn, help to extend the nuclear Periodic Table. The newly discovered nuclei are further harvested for the fundamental understanding related to various nuclear properties and the associated applications in diverse areas such as radiation, astro sciences, medical and health sector, etc.

In general, the possible target-projectile combination forms an excited compound nucleus (CN), and subsequently disintegrates into the binary fragments under various extremities, likewise excitation energy/temperature, angular momentum, deformations, orientations etc. With the effect of these factors, the de-excitation of the CN may lead to different decay mech-

anisms, viz. evaporation residues (ERs) or equivalently light-mass fragments (LFs), intermediate-mass fragment (IMF), heavy-mass fragment (HMF) and fission process. The dominance of these decay modes vary with the mass and excitation energy of CN . In the present work, we will focus on the study of fission process, which is dominant in the heavy-mass region.

The de-excitation of compound nucleus, formed via ^{208}Pb -based (cold fusion process) or ^{48}Ca -induced reactions (hot fusion process), respectively, at the low ($E_{CN}^* \approx 10-20$ MeV) [1, 2] and high excitation energies ($E_{CN}^* \approx 35-45$ MeV) [3, 4] may lead to the production of new elements. The low and high range of E_{CN}^* correspond to the incident energy $E_{c.m.}$, which may spread across the Coulomb barrier [5, 6]. In the work of Gupta and his collaborators [7], the fragmentation of excited CN has been discussed by considering quadrupole deformations along with the cold and hot optimum orientation effects. Here, the cold optimum case corresponds to the largest interaction distance between the decaying nuclear partners, which in turn gives the lowest barrier height. On the other hand, the smallest interaction distance and highest barrier height illustrates the hot op-

*jain.shivani04@gmail.com

timous case. On the basis of this criteria, the elongated (or cold) and compact (or hot) configurations of deformed nuclear partners are employed to study the fusion-fission process, respectively, at the low and high excitation energies, see Refs. [8–11]. Also, it has been investigated that, like spherical nuclei, the quadrupole deformed nuclei of closed shells are the most probable decaying fragments from compound nuclei of heavy-mass region [12–22].

Like quadrupole (β_2) deformed nuclei, the study of pear-shape octupole (β_3) deformed nuclei is equally important in order to extract the appropriate nuclear structure [23, 24]. In our recent work [25], it has been analyzed that, the octupole deformed nuclei of pear shapes which break symmetry along the reflection axis modifies the value of θ_{opt} , from the ones obtained for β_2 -deformed case. Later in a recent work [26], it has been realized that, this new set of optimum orientations related to the elongated (or cold) configuration of octupole deformed nuclei shows relatively larger impact on the fusion/Coulomb barrier, as compared to the compact (or hot) configuration case. In view of this, it would be interesting to analyze the possibility of elongated octupole deformed fission fragment emitting from a compound nucleus, which is formed at the low excitation energy.

In the recent experimental work [27], the fission dynamics of heavy-mass actinides (e.g. ^{230}Th , $^{234,236}\text{U}$, ^{240}Pu , ^{246}Cm , ^{250}Cf and ^{258}Fm) has been discussed and confirmed non-ambiguously the emission of octupole deformed nuclei/fragment of atomic number 56, i.e. ^{144}Ba , in the asymmetric region at the low excitation energy. Such analysis has motivated us to study the application of cold optimum orientations of octupole deformed fragments in the fission dynamics of even-even isotopes of Th, i.e. $^{222-230}\text{Th}^*$. This analysis is exercised at the low value of E_{CN}^* , which corresponds to the cold synthesis of element. To carry forward with this idea, we are using the Dynamical Cluster-decay Model (DCM) [28–30], which is applied to probe various decay mechanisms of CN formed in heavy-ion induced reactions. The model has been built-on the collective clusterization approach of Quantum Mechanical Fragmentation Theory (QMFT) [31–33].

In the present work, to have an explicit understanding of higher-order deformation (up to β_3) and related cold optimum orientations, the fission of Th isotopes is discussed by a comparative analysis of fission fragment distributions using mass asymmetry (η_A) and charge asymmetry (η_Z) parameters. In the above analysis, the minima of potential observed in the fission region helps in determining the peak value of preformation probability for the fission fragments. On the basis of this, the identification of the most probable fission fragments in reference to η_A and η_Z -coordinates is also done. Note that, the neck-length parameter optimized for $^{224}\text{Th}^*$ nucleus in reference to the available experimental data for the below-barrier energies [34] has been worked out for the fragmentation analysis of the remaining isotopes of Th. In DCM, the neck-length parameter ΔR , the only parameter, is uti-

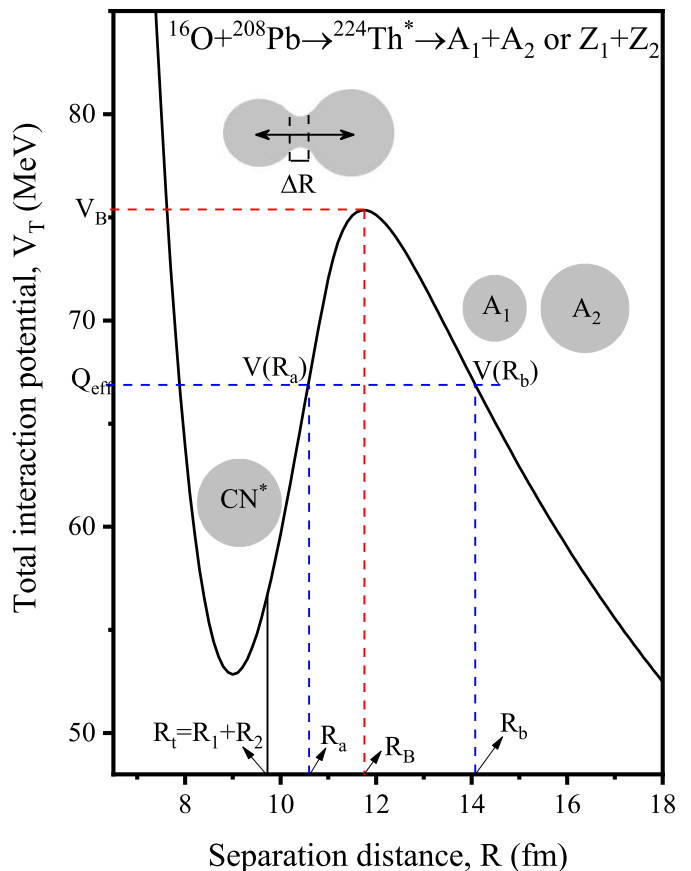


FIG. 1: The variation of total interaction potential V_T (MeV) as a function of separation distance R (fm) between the colliding nuclear partners is shown for $^{16}\text{O} + ^{208}\text{Pb} \rightarrow ^{224}\text{Th}^*$ reaction. Here, $R_a = R_1(\alpha_1, T) + R_2(\alpha_2, T) + \Delta R$ defines the first turning point.

lized to fix the first turning point, where the preformed fragments start to penetrate through the interaction potential. In relevance to the study undertaken, Section II describes the collective clusterization approach of DCM. In Section III, a detailed discussion is made on the results obtained by incorporating the deformations up to β_3 with cold optimum orientation effects. Finally, a brief summary is given in Section IV.

II. METHODOLOGY

A. The dynamical cluster-decay model (DCM)

In the present work, the decay of excited compound nuclei (CN) has been studied using the collective clusterization approach of dynamical cluster-decay model (DCM) [28–30]. The model is derived using collective co-ordinates of mass (and charge) asymmetry parameter $\eta_A = \frac{|A_1 - A_2|}{A_1 + A_2}$ [and $\eta_Z = \frac{|Z_1 - Z_2|}{Z_1 + Z_2}$] (here 1 and 2 correspond to the decaying binary fragments), relative separation distance R , nuclear deformations β_{λ_i} ($\lambda = 2, 3$;

$i = 1, 2$), and orientation (θ_i), etc. Depending on these co-ordinates, the fission cross-section of decaying fragments is given as

$$\sigma_{fis}(A_1, A_2) = \frac{\pi}{k^2} \sum_{\ell=0}^{\ell_{max}} (2\ell + 1) P_0 P, \quad (1)$$

here, the fission fragments decaying from considered Th isotopes of the mass/charge-symmetric and asymmetric regions have mass and charge numbers of $A_2 = \frac{A_{CN}}{2} \pm 35$ and $Z_2 = \frac{Z_{CN}}{2} \pm 15$ ranges, respectively. Note that, A_{CN} and Z_{CN} are the mass and charge numbers of compound nucleus, respectively. $k = \sqrt{\frac{2\mu E_{c.m.}}{\hbar^2}}$ and $\mu = m[A_1 A_2 / (A_1 + A_2)]$ is the reduced mass. ‘m’ is the nucleon mass. In the above expression, the term ‘ P_0 ’ is the preformation probability which contains the structural information of the compound nuclear system. Based on the QMFT, the P_0 is calculated by solving the stationary Schrodinger equation in η -coordinates [35]

$$\left\{ -\frac{\hbar^2}{2\sqrt{B_{\eta\eta}}} \frac{\partial}{\partial \eta} \frac{1}{\sqrt{B_{\eta\eta}}} \frac{\partial}{\partial \eta} + V_R(\eta, T) \right\} \psi^\nu(\eta) = E^\nu \psi^\nu(\eta), \quad (2)$$

here $\nu = 0$ refers to the ground state and $\nu = 1, 2, 3, \dots$ correspond to the excited states. Note that, in the above equation, η can be mass (η_A) or charge (η_Z) dependent, and subsequently, the solution of Eq.(2) gives P_0 as a function of mass-asymmetry parameter η_A [36],

$$P_0(\eta_A) = |\psi(\eta(A_i))|^2 \sqrt{B_{\eta_A \eta_A}} \frac{2}{A_{CN}}. \quad (3)$$

On the other hand, the preformation probability as a function of charge-asymmetry parameter η_Z reads as [37]

$$P_0(\eta_Z) = |\psi(\eta(Z_i))|^2 \sqrt{B_{\eta_Z \eta_Z}} \frac{2}{Z_{CN}}. \quad (4)$$

In Eqs.(3) and (4), the states $\psi(\eta(A_i))$ and $\psi(\eta(Z_i))$, respectively, are the vibrational states. For fission from excited states, the possible outcomes related to the excitations of higher vibrational states are considered by assuming them as Boltzmann-like wave function, such as

$$|\psi|^2 = \sum_{\nu=0}^{\infty} |\psi^\nu|^2 \exp(E^\nu/T). \quad (5)$$

In the above equations, $B_{\eta_A \eta_A}$ and $B_{\eta_Z \eta_Z}$ are the smooth hydro-dynamical parameters, for more details see [38]. In Eq.(1), the other term ‘ P ’ is called as the penetration probability. This means the preformed cluster/fragment formed inside the potential pocket starts penetrating through the first classical turning point, i.e. $R = R_a = R_1(\alpha_1, T) + R_2(\alpha_2, T) + \Delta R$, and terminates through the second turning point R_b , such that $V(R_a) = V(R_b)$, for clarity see Fig.1, where total interaction potential is plotted as a function of separation distance. The idea of introducing neck-length parameter

ΔR within the DCM [40–42] is similar to that of saddle [43, 44] and scission-point [45] statistical fission model. The permissible value of ΔR lies in the nuclear proximity range of about 2 fm, since the surface interaction between two fragments can take place around this range of ΔR to experience the nuclear force.

The term P in Eq.(1) is calculated using the WKB approximation and given as [39]

$$P = \exp \left[-\frac{2}{\hbar} \int_{R_a}^{R_b} \{2\mu[V(R) - Q_{eff}]\}^{1/2} dR \right]. \quad (6)$$

In the above equation, ‘ Q_{eff} ’ is the effective Q -value of the decay channel.

In solving the Schrodinger equation, see Eq.(2), a term $V_R(\eta, T)$ involved defined as the fragmentation potential is given as

$$V_R(\eta, T) = \sum_{i=1}^2 [V_{LDM}(A_i, Z_i, T)] + \sum_{i=1}^2 [\delta U_i] \exp(-T^2/T_0^2) + V_C(R, Z_i, \beta_{\lambda i}, \theta_i, T) + V_\ell(R, A_i, \beta_{\lambda i}, \theta_i, T) + V_N(R, A_i, \beta_{\lambda i}, \theta_i, T). \quad (7)$$

Here, V_{LDM} considered is the temperature-dependent liquid drop model (LDM) of Davidson *et al* [46, 47]. For relevant details see Ref. [48]. The second term i.e. shell-corrections is given by Myer and Switecki [49] with its T -dependence from Davidson *et al* [46]. The constituents of total potential, such as Coulomb potential (V_C), centrifugal potential (V_ℓ) and nuclear proximity potential (V_N), are function of relative separation distance R , charge Z_i (mass A_i) number, temperature T , deformations $\beta_{\lambda i}$ and orientation θ_i degrees of freedom.

For spherical-deformed or deformed-deformed combinations, the repulsive Coulomb potential for coplanar oriented nuclei is given by [50]

$$V_C(R, Z_i, \beta_{\lambda i}, \theta_i, T) = \frac{Z_1 Z_2 e^2}{R} + 3Z_1 Z_2 e^2 \sum_{i=1,2} \sum_{\lambda=2,3} \frac{1}{2\lambda+1} \frac{R_i^\lambda(\alpha_i, T)}{R(T)^{\lambda+1}} \times Y_\lambda^{(0)}(\theta_i) \left[\beta_{\lambda i} + \frac{4}{7} \beta_{\lambda i}^2 Y_\lambda^{(0)}(\theta_i) \right], \quad (8)$$

where $Y_\lambda^{(0)}(\theta_i)$ and $R_i(\alpha_i)$ represent the spherical harmonic functions and nuclear radius term, respectively. $\lambda = 2, 3$ stands for quadrupole and octupole deformations, respectively. The deformations of the nuclei, belonging to different mass-region are taken from the data table of Möller *et al* [51]. The multipole expansion of the nuclear radius of deformed nuclei $R_i(\alpha_i)$ is described in terms of the spherical harmonic function [52, 53], as given below

$$R_i(\alpha_i, T) = R_{0i}(T) \left[1 + \sum_{\lambda=2,3} \beta_{\lambda i} Y_\lambda^{(0)}(\alpha_i) \right]; \quad (9)$$

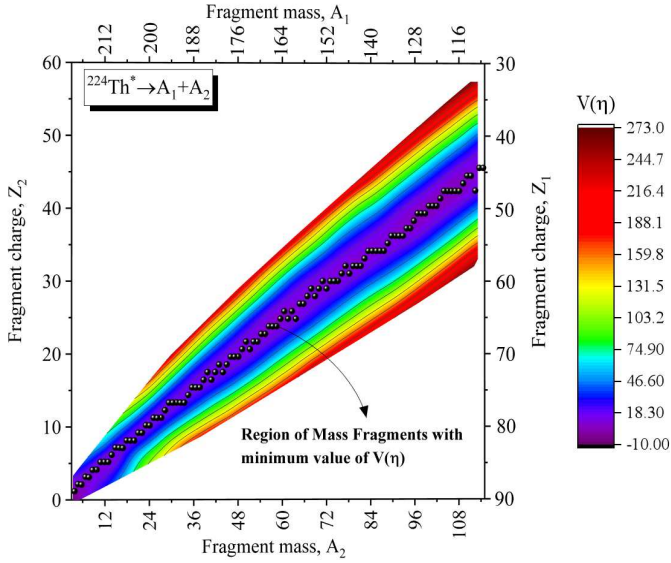


FIG. 2: The color-map representing the fragmentation potential $V(\eta)$ for $^{224}\text{Th}^*$ with respect to the fragment mass number A_2 having isobars (of different charge number Z_2). The mass A_1 and charge number Z_1 of decaying partner are also shown in the top and right axes, respectively.

in the above expression, the T -dependent nuclear radius term $R_{0i}(T)$ is given as [54]

$$R_{0i}(T) = R_{0i}[1 + 0.0005T^2]. \quad (10)$$

Here, $R_{0i}(= 1.28A_i^{1/3} - 0.76 + 0.8A_i^{-1/3})$ in fm [55] represents the radius of the equivalent spherical nucleus. The temperature T is related to the excitation energy E_{CN}^* of the compound nucleus and given as [56]

$$E_{CN}^* = E_{c.m.} + Q_{in} = \frac{A_{CN}}{9}T^2 - T. \quad (11)$$

The rotational energy is given as [50]

$$V_\ell(R, A_i, \beta_{\lambda i}, \theta_i, T) = \frac{\hbar^2 \ell(\ell + 1)}{2I(T)}. \quad (12)$$

The nuclear proximity potential (V_N) is obtained from Blocki *et al* [55]. Here, a collective formulation for deformed and coplanar oriented nuclei is considered [57–60], and V_N reads as

$$V_N(A_i, \beta_{\lambda i}, \theta_i, T) = 4\pi \bar{R}(T) \gamma b(T) \phi(s_0). \quad (13)$$

Note that, V_N is a product of two terms, one $[4\pi \bar{R}(T) \gamma b(T)]$ depends on the shape and geometry (relative orientation) of colliding nuclei, another term $[\phi(s_0)]$ is a function of single parameter, that is the minimum separation distance (s_0) between two colliding surfaces.

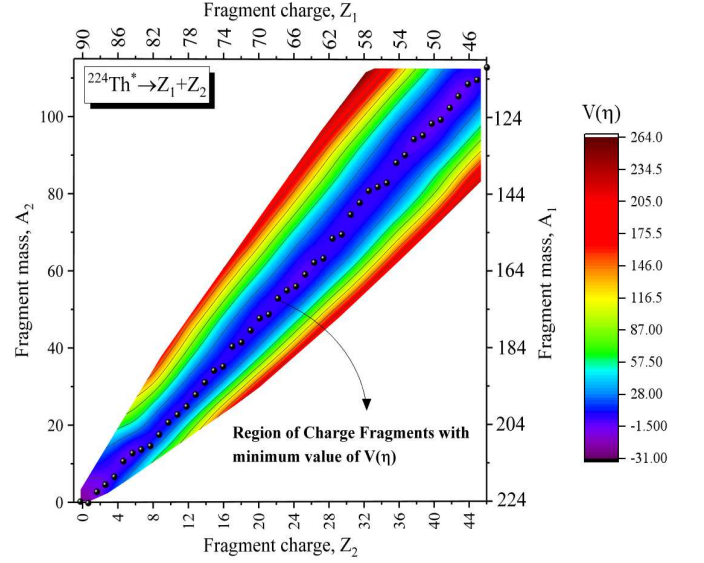


FIG. 3: The color-map representing the fragmentation potential for $^{224}\text{Th}^*$ with respect to the fragment charge number Z_2 having isotopes (of different mass number A_2).

III. RESULTS AND DISCUSSION

In the present work, the main purpose is to analyze the influence of elongated (or cold) configuration of octupole (β_3) deformed nuclei in the fission dynamics of even-even isotopes of Thorium, i.e. $^{222-230}\text{Th}^*$. The calculations are done at the low value of excitation energy E_{CN}^* which is relevant for the cold synthesis process. To carry forward with this idea, the deformations (up to β_3) and corresponding cold optimum orientation [25] are included in the framework of the Dynamical Cluster-decay Model (DCM), which is developed on the basis of Quantum Mechanical Fragmentation Theory (QMFT). In the notion of QMFT, the probable decaying fragments/cluster are pre-born inside the excited Compound Nucleus (CN) and then they penetrate through the interaction potential. With the use of the neck-length parameter ΔR , which is the only parameter of DCM, one can fix the turning point of the barrier penetration.

To have the knowledge of the turning points for pre-born fragments of Th^* isotopes, the neck-length parameter has to be optimized first, in view of the fission data at the low excitation energies, corresponding to the below-barrier energies. In view of this, Section III A explores the fission cross-sections by including deformations (up to β_3) and cold optimum orientation effects in DCM for $^{224}\text{Th}^*$ compound nucleus and compared the results with available experimental data [34]¹. Further, in Section III B, the de-

¹ Note that, for below-barrier region, the experimental measurements of fission cross-sections are available only for $^{16}\text{O} + ^{208}\text{Pb} \rightarrow ^{224}\text{Th}^*$ reaction.

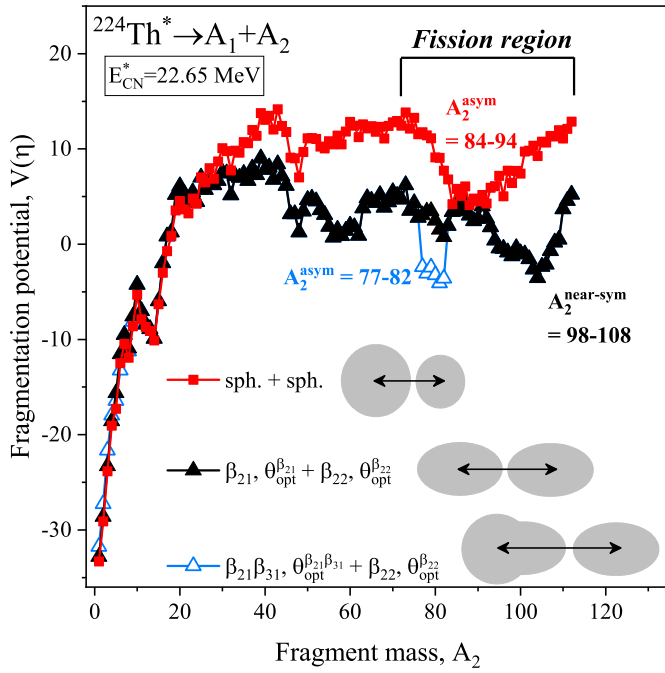


FIG. 4: (Color online) The variation of minimized fragmentation potential with respect to the mass number of decaying fragment, firstly for spherical (sph.) and then by including quadrupole (β_{2i}) and octupole (β_{3i}) deformations along with the related cold optimum orientations ($\theta_{opt}^{\beta_{\lambda=2,3}}$). Here, $i=1, 2$ refer to binary fragments A_1 and A_2 , respectively.

cay analysis of $^{222,224,226,228,230}\text{Th}^*$ nuclei is illustrated at the same neck-length ΔR , obtained in fitting the data for $^{16}\text{O}+^{208}\text{Pb}$ reaction forming $^{224}\text{Th}^*$ compound nucleus. The above analysis is discussed in terms of the fragmentation potential ($V(\eta)$), which is minimized in reference to the mass (A_2) and charge number (Z_2) of decaying fragment. Subsequently, the preformation probability P_0 (showing the inverse trend of $V(\eta)$) as a function of mass- (η_A) and charge-asymmetry (η_Z) coordinates illustrates, respectively, the mass- and charge-dispersion cases.

A. Fission cross-sections for $^{224}\text{Th}^*$ nucleus formed in ^{208}Pb -based reaction

The minimization of fragmentation potential can be done in reference to the mass number A_2 as well as charge number Z_2 of decaying nuclear partner from $^{224}_{90}\text{Th}^*$ and can be understood from Figs. 2 and 3, respectively. In Fig. 2, the mass number A_2 of fragment and its isobars of different charge number Z_2 are shown along the horizontal and vertical axes, respectively. The color-map represents the strength of fragmentation potential $V(\eta)$ for each A_2 and corresponding Z_2 . The black spheres in the dark purple region show the lowest or minimum value of $V(\eta)$ for the decay fragments, which helps in choosing Z_2 for corresponding A_2 values. In other words, it is

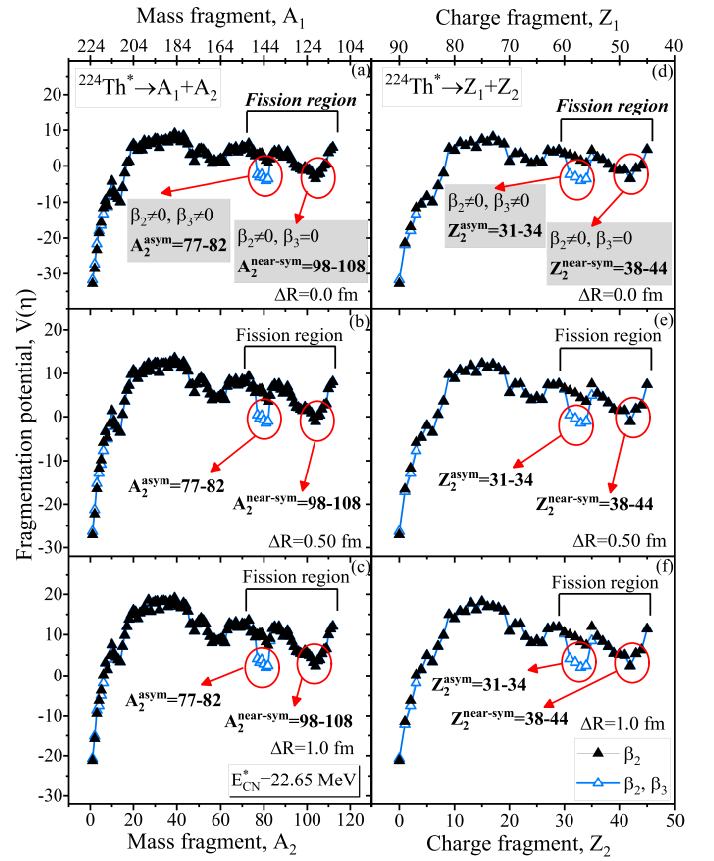


FIG. 5: (Color online) The minimized fragmentation potential in reference to the fragment (a)-(c) mass A_2 and (d)-(f) charge number Z_2 of $^{224}\text{Th}^*$, at low excitation energy $E_{CN}^* = 22.65$ MeV and $\ell = 0\hbar$. The analysis is exercised at different values of neck-length parameter, i.e. $\Delta R = 0.0, 0.5$ and 1.0 fm.

called the minimization of fragmentation potential in reference to the mass number of CN . Further in Fig. 3, for each Z_2 of decay fragment, there are isotopes of different mass number A_2 and the spherical dots present in the dark blue color indicate the minima of $V(\eta)$ for an isotope. This way, one can find the minimization of $V(\eta)$ in reference to the charge number. Note that, the mass and charge numbers of other decay partner are $A_1 = A - A_2$ and $Z_1 = Z - Z_2$, respectively, as shown in the opposite axes of A_2 and Z_2 of Figs. 2 and 3.

Further, the minimized potential $V(\eta)$ obtained for the disintegration of $^{224}\text{Th}^*$ over the fragment mass $A_1 = 1-223$ (and $A_2 = 223-1$) and charge number $Z_1 = 0-90$ (and $Z_2 = 90-0$) is discussed to understand the fragmentation structure with the inclusion of deformations (up to β_3) and cold optimum orientation effects. For an illustration, in Fig.4, the role of quadrupole/octupole deformations and associated cold optimum orientation can be analyzed in reference to the spherical configuration of decaying fragments in the fission valley/region (marked in the figure). This region has the mass range of fission fragment A_2 from 72 to 112. It is clearly seen from this

TABLE I: The detail of calculated fission cross-sections σ_{fis}^{DCM} (mb) of $^{16}\text{O}+^{208}\text{Pb}\rightarrow^{224}\text{Th}^*$ reaction with the inclusion of deformation up to β_3 and related cold optimum orientation ($\theta_{opt}^{\beta_2}$ and $\theta_{opt}^{\beta_2,\beta_3}$). For comparison, the experimental data [34] of the above mentioned reaction is also given.

E_{CN}^* (MeV)	$E_{c.m.}$ (MeV)	T (MeV)	$\sigma_{fis}^{Expt.}$ (mb)	ΔR (fm)		$\ell_{max}(\hbar)$		σ_{fis}^{DCM} (mb)	
				β_2	β_2, β_3	β_2	β_2, β_3	β_2	β_2, β_3
$^{224}\text{Th}^* \rightarrow A_1 + A_2$									
22.65	68.69	0.974	0.00844±0.0035	0.80	0.81	92	104	0.00649	0.00845
23.46	69.49	0.991	0.04624±0.0145	0.81	0.87	95	105	0.0438	0.0431
24.37	70.41	1.009	0.4869±0.137	0.98	1.05	95	105	0.452	0.491
25.29	71.33	1.028	2.1503±0.634	1.00	1.08	98	108	2.201	2.0464
$^{224}\text{Th}^* \rightarrow Z_1 + Z_2$									
22.65	68.69	0.974	0.00844±0.0035	0.25	0.30	111	123	0.00545	0.00866
23.46	69.49	0.991	0.04624±0.0145	0.28	0.35	116	125	0.0428	0.0361
24.37	70.41	1.009	0.4869±0.137	0.42	0.48	118	126	0.305	0.335
25.29	71.33	1.028	2.1503±0.634	0.55	0.56	120	132	1.504	2.595

figure that, as one goes from spherical (sph.)+sph. to quadrupole (quad.)+quad. and then to quad.+octupole deformed pairs of decay fragments, the interaction distance increases, which in turn, lowers the potential barrier with a larger extent. As a consequence, one can see that, the minimization and structure of fragmentation potential modifies with a significant effect due to incorporation of deformation and orientation degrees of freedom.

Later, in the comparative analysis of mass- and charge-dispersion cases, the behavior of $V(\eta)$ has been tested for different values of neck-length parameter ΔR (=0.0, 0.5 and 1.0 fm), as shown in Fig.5. The above analysis is exercised at the lowest value of excitation energy, i.e. $E_{CN}^*=22.35$ MeV, which is referred from the available experimental data of fission cross-sections for $^{16}\text{O}+^{208}\text{Pb}\rightarrow^{224}\text{Th}^*$ reaction at energies 22.65-25.29 MeV [34]. Since the present work is constrained to study the fission process of above mentioned reaction, so the relevant dips are specified in Fig.5 for fragmentation potential. One can clearly see the dip of $V(\eta)$ near the symmetric region ($\approx \frac{A_{CN}}{2}=112$ and $\frac{Z_{CN}}{2}=45$) for quadrupole (β_2) deformed nuclei associated with the cold optimum orientation. Afterwards, the presence of octupole (β_2, β_3) deformed fragments along with the optimum orientation defining its elongated configuration show the minima of $V(\eta)$ in the asymmetric region which competes with that of the near-symmetric region. Also, it is important to note that, the magnitude and structure of potential observed in both the mass and charge distributions of $^{224}\text{Th}^*$ is almost similar. The above results obtained due to β_2, β_3 -deformations and related cold optimum orientations are consistently true for different choices of ΔR . In the calculation of preformation probability P_0 , the mass- and charge-dispersion concepts

are introduced through the mass- ($\eta_A = \frac{|A_1-A_2|}{A_1+A_2}$) and charge-asymmetry ($\eta_Z = \frac{|Z_1-Z_2|}{Z_1+Z_2}$) coordinates, which are treated as the dynamical factors in the collective clusterization approach of DCM. It is known that, the decaying binary fragments with the minimum value of fragmentation potential possess the highest preformation probability P_0 . In other words, it can be said that, the term ' P_0 ' shows an inverse trend from that of $V(\eta)$ observed in Fig.5. The fission fragments observed in the near-symmetric and asymmetric regions in both the mass- and charge-distribution cases are almost similar.

On the basis of above observation, we have calculated the fission cross-sections (σ_{fis}^{DCM}) using DCM for both the mass- and charge-distributions of $^{224}\text{Th}^*$, formed from $^{16}\text{O}+^{208}\text{Pb}$ reaction, at energies below the Coulomb barrier. The detail of theoretically and experimentally obtained σ_{fis} for the above mentioned reaction is given in Table I. The calculations have been done initially with the inclusion of β_2 -deformation and related cold optimum orientation ($\theta_{opt}^{\beta_2}$). Subsequently, the experimental data has been addressed within the permissible values of ΔR , for incident beam energies $E_{c.m.}=68.69 - 71.33$ MeV. In the above calculations, the values of ℓ_{max} are obtained at a point when there is no contribution of light particle. Later, due to involvement of deformations (up to β_3) along with $\theta_{opt}^{\beta_2,\beta_3}$, there is an increment of in ℓ_{max} about 10% and the obtained σ_{fis}^{DCM} are found closer to $\sigma_{fis}^{Expt.}$. However, there is a very small change in ΔR . Apart from this, one can also notice from Table I that, the neck-length parameter reduces significantly, as one moves from the mass-distribution to the charge-distribution criteria. This means, for charge-dispersion case, the interaction among decaying fragments takes place at relatively smaller distance from that of the mass-

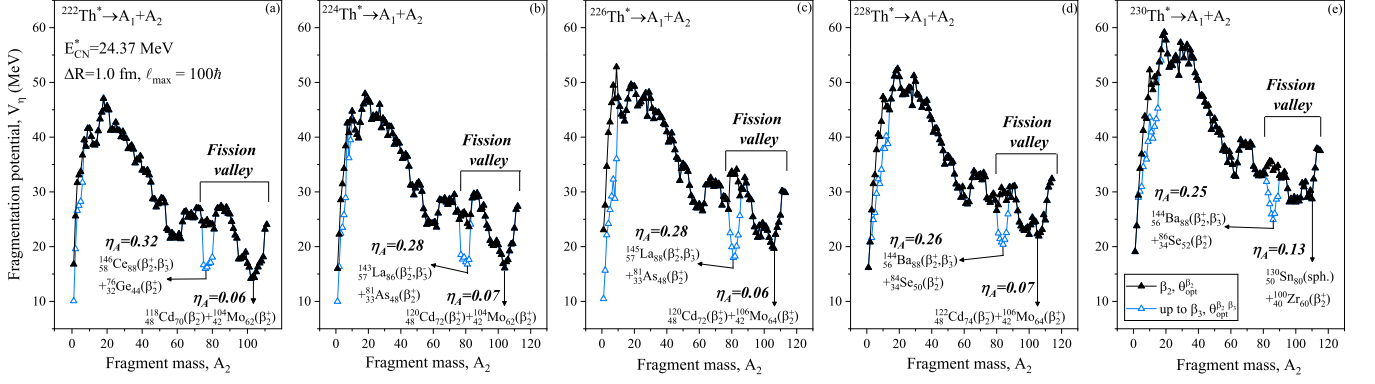


FIG. 6: (Color online) The variation of fragmentation potential $V(\eta)$ is plotted as a function of mass number A_2 firstly with the inclusion of quadrupole β_2 deformation (and related cold optimum orientation $\theta_{opt}^{\beta_2}$) and secondly octupole β_3 deformation (and $\theta_{opt}^{\beta_3}$) of decaying fragment being involved for the decay analysis of even-even isotopes of $^{222-230}\text{Th}^* \rightarrow A_1 + A_2$, at a common excitation energy $E_{CN}^* = 24.37$ MeV.

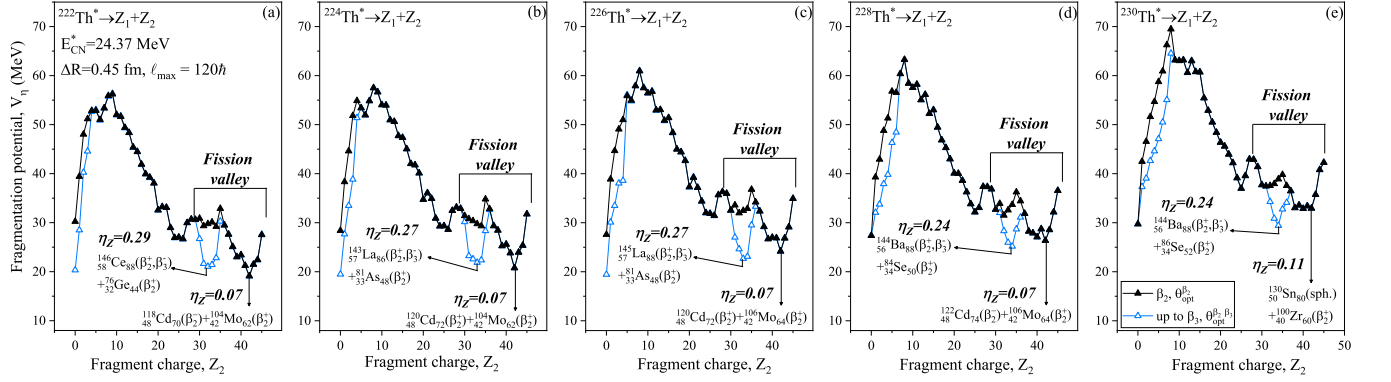


FIG. 7: (Color online) Same as Fig.6, but the variation of $V(\eta)$ is shown with respect to charge number Z_2 of even-even isotopes of $^{222-230}\text{Th}^* \rightarrow Z_1 + Z_2$.

dispersion/distribution of an excited compound nucleus. Based on the above observations related to the neck-length parameter and ℓ_{max} -values, the fission dynamics of all considered isotopes of $^{222,224,226,228,230}\text{Th}^*$ has been studied using DCM. There is a very small difference in ΔR and ℓ_{max} -values, while studying the fission dynamics of isotopes of a compound nucleus [61, 62]. Thus, for decay analysis of even-even isotopes of $^{222-230}\text{Th}^*$ via mass-distribution at $E_{CN}^* = 24.37$ MeV, we have considered common $\Delta R = 1.0$ fm and $\ell_{max} = 100 \hbar$, using the systematic of ^{224}Th compound nucleus. Similarly, for charge-distribution which takes place comparatively at smaller distance, like $\Delta R = 0.45$ fm and $\ell_{max} = 120 \hbar$ values can be taken into account.

B. Mass and charge dispersion of even-even isotopes of $^{222-230}\text{Th}^*$

The study based on the fusion-fission phenomena is not only for the calculation of fission cross-section, but it also provides the idea of symmetric/asymmetric mass and charge fragments produced during the disintegration

of an excited CN . In view of this, the structure of fragmentation potential $V(\eta)$ is shown in Fig. 6 with respect to the mass number A_2 of decaying fragment from $^{222,224,226,228,230}\text{Th}^*$. The region of interest that is the fission valley is marked in this figure. Interestingly, two minima are observed in the fragmentation potential for each considered isotopes of Th which belong to near-symmetric and asymmetric mass region. The near mass-symmetric region corresponds to the quadrupole (β_2) deformed fragments of elongated configuration. Whereas, the presence of octupole deformation in one of the decaying nuclear partner minimizes the fragmentation potential in the mass-asymmetric region ($\eta_A \approx 0.3$). Moreover, one can notice in Fig. 6(a) for $^{222}\text{Th}^*$ that, the near-symmetric fission shows deeper minima in $V(\eta)$ as compared to the asymmetric fission fragments. For $^{224}\text{Th}^*$ case represented in Fig. 6(b), the minima of $V(\eta)$ observed in the asymmetric fission starts competing with the near-symmetric dip. Moving ahead, a transition is observed for heavy-mass isotopes, i.e. $^{226,228,230}\text{Th}^*$, as shown in panels (c)-(e) of Fig.6. In other words, the minima in $V(\eta)$ becomes relatively deeper for octupole deformed fragments present in the asymmetric region, than

TABLE II: The detail of the most probable fission fragments of quadrupole (β_{2i} ; here $i=1, 2$) and octupole deformation (β_{3i}) along with their related cold optimum orientations ($\theta_{opt}^{\beta_2}$ [7] and $\theta_{opt}^{\beta_2\beta_3}$ [25]) found respectively in the near mass/charge-symmetric and asymmetric fission regions of even-even isotopes of $^{222-230}\text{Th}^*$ compound nuclei are listed in the following table.

CN^*	Near mass/charge-symmetric region					Mass/charge-asymmetric region						
	Fission fragments	β_{21}	β_{22}	$\theta_{opt}^{\beta_{21}}$	$\theta_{opt}^{\beta_{22}}$	Fission fragments	β_{21}	β_{31}	β_{22}	β_{32}	$\theta_{opt}^{\beta_{21}\beta_{31}}$	$\theta_{opt}^{\beta_{22}\beta_{32}}$
$^{222}\text{Th}^*$	$^{118}_{48}\text{Cd}_{70} + ^{104}_{42}\text{Mo}_{62}$	-0.238	0.377	90°	180°	$^{146}_{58}\text{Ce}_{88} + ^{76}_{32}\text{Ge}_{44}$	0.182	-0.116	0.143	0.0	0°	180°
$^{224}\text{Th}^*$	$^{120}_{48}\text{Cd}_{72} + ^{104}_{42}\text{Mo}_{62}$	0.140	0.377	0°	180°	$^{143}_{57}\text{La}_{86} + ^{81}_{33}\text{As}_{48}$	0.154	-0.104	0.163	0.0	0°	180°
$^{226}\text{Th}^*$	$^{120}_{48}\text{Cd}_{72} + ^{106}_{42}\text{Mo}_{64}$	0.140	0.377	0°	180°	$^{145}_{57}\text{La}_{88} + ^{81}_{33}\text{As}_{48}$	0.173	-0.128	0.163	0.0	0°	180°
$^{228}\text{Th}^*$	$^{122}_{48}\text{Cd}_{74} + ^{106}_{42}\text{Mo}_{64}$	-0.104	0.354	90°	180°	$^{144}_{56}\text{Ba}_{88} + ^{84}_{34}\text{Se}_{50}$	0.164	-0.126	0.053	0.0	0°	180°
$^{230}\text{Th}^*$	$^{130}_{50}\text{Sn}_{80} + ^{100}_{40}\text{Zr}_{60}$	0.00	0.364	0°	180°	$^{144}_{56}\text{Ba}_{88} + ^{86}_{34}\text{Se}_{52}$	0.164	-0.126	0.125	0.0	0°	180°

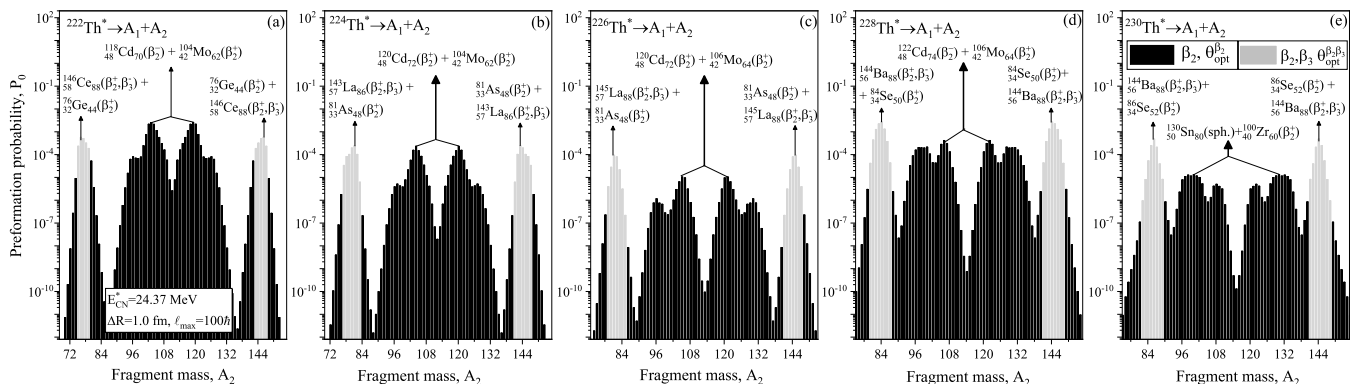


FIG. 8: The variation of preformation probability ' P_0 ' as a function of mass number of decaying fragment (A_2) from the even-even isotopes of $^{222-230}\text{Th}^* \rightarrow A_1 + A_2$ is shown firstly with the inclusion of quadrupole β_2 deformation and related optimum orientation ($\theta_{opt}^{\beta_2}$) and secondly higher-order deformations (up to β_3) and $\theta_{opt}^{\beta_3}$ being involved.

that of near-symmetric quadrupole deformed fragments. Similar results have been observed while studying the 'charge-dispersion' of even-even isotopes of $^{222-230}\text{Th}^*$, as shown in panels (a)-(e) of Fig.7. Note that, from both the mass- and charge-dispersion cases, the fission fragments observed at deep valley location are identical.

In Table II, we have shown the atomic and neutron numbers, respectively at the left and right subscripts, of near-symmetric and asymmetric fission fragments along with their quadrupole (β_{2i}), octupole (β_{3i}) deformations and related cold optimum orientations ($\theta_{opt}^{\beta_2}$ and $\theta_{opt}^{\beta_2\beta_3}$). It is known that, the minimization in fragmentation potential occurs due to shell stabilization, which generally comes for magic number of nucleons, either in one or both the fission fragments. On the basis of this fact, it has been analyzed in the near-symmetric region that, the fission fragments are quadrupole deformed and one of them in decaying from light mass isotopes of Th ($^{222,224}\text{Th}^*$) has neutron number equal to 62, which is a deformed magic number and provides shell stabilization [22]. On the other hand, in the asymmetric fission region of heavy-mass isotopes ($^{226,228,230}\text{Th}^*$), the decaying fragment of

upto octupole deformation has atomic number close or equal to 56. In the recent experimental works [24, 27, 63], it has been shown that, the nucleus of atomic number 56 (of ^{156}Ba element) or close to it possessing octupole deformation gives extra stability. Due to these facts, one can see minimization in $V(\eta)$ with prominent effect. In addition to the above, one can also notice from Table II that, in near-symmetric region, the magnitude of β_{21} for fragment A_1 is decreasing and becomes zero, as one goes from $^{224}\text{Th}^*$ to $^{230}\text{Th}^*$ case. On the other hand, in the asymmetric region, one of decay fragments is octupole deformed and another is quadrupole deformed. Here, the magnitude of β_{31} is relatively larger for fragment A_1 of heavy-mass isotopes of Th ($^{226,228,230}\text{Th}^*$), as compared to that of light-mass isotopes. In our recent work [26], it has been said that, for larger magnitude of β_3 , the elongated configuration of octupole deformed nuclei enlarges the interaction distance with a large extent and gives relatively lower barrier height. As a consequence, one can notice the corresponding effects in the fragmentation potential. From above analysis, one can notice that, the presence of deformations as well as shell-stabilization

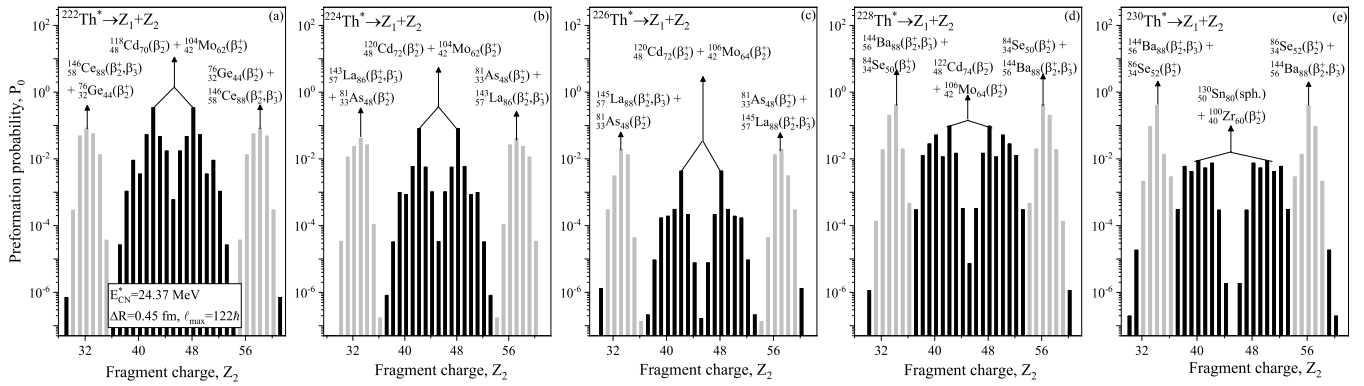


FIG. 9: Same as Fig.8, but for the charge dispersion case, i.e. $^{222-230}\text{Th}^* \rightarrow Z_1 + Z_2$.

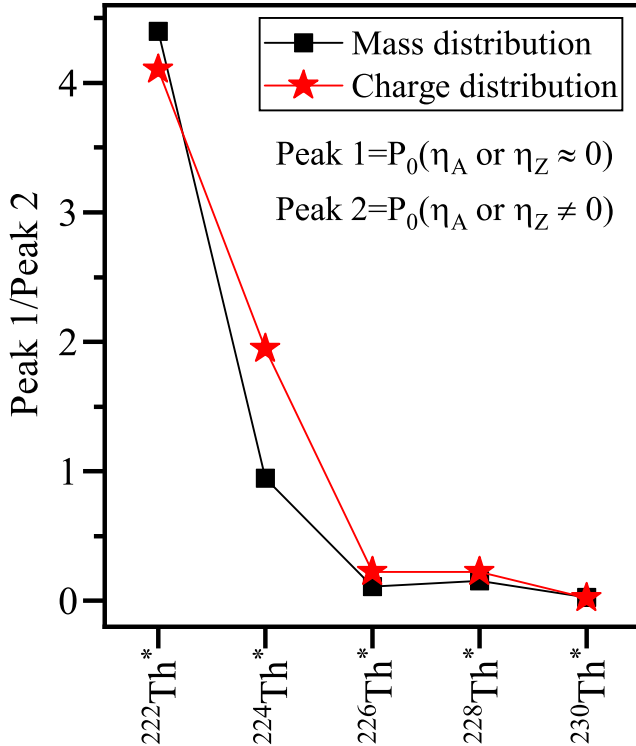


FIG. 10: The ratio of Peak 1 [$=P_0(\eta_A \text{ or } \eta_Z \approx 0)$] and Peak 2 [$=P_0(\eta_A \text{ or } \eta_Z \neq 0)$] obtained for even-even isotopes of $^A\text{Th}^*$, here $A=222, 224, 226, 228$ and 230 , at a common excitation energy, $E_{CN}^*=24.37$ MeV.

(due to magicity in nucleon number) play a significant role in the fission valley of Th.

Further, the role of deformation and orientation effect has been explored in the calculation of preformation probability P_0 as a function of mass and charge number of fission fragments preformed inside the even-even isotopes of $^{222-230}\text{Th}^*$, at a common excitation energy $E_{CN}^*=24.37$ MeV. It is known that, the fragments for which the fragmentation potential gets minimized have the highest preformation probability. In a recent work [64], a transition

of symmetric to asymmetric fission has been shown, as one moves from ^{222}Th to ^{230}Th compound nuclei. Additionally, in Ref.[65], the charge distribution of $^{222,224}\text{Th}$ isotopes shows a rise in the asymmetric region, but lower than symmetric fission, for excitation energy more than 11 MeV. Our calculations are in agreement with these observations. To show this, the preformation probability (P_0) of even-even isotopes of $^{222-230}\text{Th}^*$ are discussed and also shown in Figs. 8 and 9 respectively for mass- and charge-dispersion cases. It is clear from these figures that, the octupole deformed nuclei always appear in the asymmetric mass regions, irrespective of the choice of mass and excitation energy range considered in the present work. In the above analysis, the near-symmetric fission is found dominant over asymmetric fission for $^{222}\text{Th}^*$ case, at $E_{CN}^*=24.37$ MeV. For $^{224}\text{Th}^*$, the contribution of near-symmetric and asymmetric components is comparable. On the other hand, for heavy-mass isotopes $^{226,228,230}\text{Th}^*$, the octupole deformed decaying nuclear partner of atomic number equal or close to 56 (^{145}La and ^{144}Ba) in asymmetric region shows dominant behavior. In other words, it can be said that, the asymmetric fission fission fragments of octupole-quadrupole deformed kind ($^{145}\text{La}+^{81}\text{As}$, $^{144}\text{Ba}+^{84}\text{Se}$ and $^{144}\text{Ba}+^{86}\text{Se}$) enhances the preformation probability P_0 with a larger extent. Also, in a recent experimental work [27], the authors have given the evidence of pear-shape nuclei (i.e. ^{144}Ba) in asymmetric region of heavy-mass actinides and the present work is in line with the result of this paper.

Further, the ratio of preformation probability P_0 peaks obtained near the symmetric region (Peak 1) and the one in the asymmetric region (Peak 2) is shown in Fig.10 for $^{222,224,226,228,230}\text{Th}^*$ fission nuclei. In this figure, the ratio ($\frac{\text{Peak1}}{\text{Peak2}}$) is obtained for both the mass- as well as charge-distributions of above said compound nuclei. It is observed that, the peak ratio decreases with increase in mass number of compound nuclei. Clearly, the lighter-mass compound nuclei prefer near-symmetric fragmentation of quadrupole-quadrupole deformed pairs of fission fragments. However, asymmetric fission of octupole-quadrupole deformed fragments is prominent in the heavier isotopes, i.e. $^{226,228,230}\text{Th}^*$.

IV. SUMMARY

In this paper, we have included the deformations up to β_3 and related cold optimum orientation (θ_{opt}), within the Dynamical Cluster-decay Model, to study the nuclear fission dynamics of even-even isotopes of Thorium, i.e. $^{222-230}\text{Th}^*$. The above analysis is exercised at the low excitation energy, which corresponds to the cold optimum configurations of the nuclei involved.

Initially, the neck-length parameter ΔR is optimized in reference to the available experimental data of fission cross-sections of $^{224}\text{Th}^*$, formed via ^{208}Pb -based reaction, at the below-barrier energies. Subsequently, the dips of fragmentation potential and corresponding peaks of preformation probability are analyzed in the near-symmetric (η_A and $\eta_Z \approx 0$) and asymmetric fission (η_A and $\eta_Z \neq 0$) regions of considered isotopes. It is observed that octupole deformed fragments appear in the asymmetric region, irrespective of the mass of Th isotopes. Note that, for both the mass- as well as charge-dispersion fragmentations, the most probable fission fragments observed are found identical. In the decay of light-mass isotopes of Th, i.e. $^{222,224}\text{Th}^*$, the near-symmetric fission is preferred due to deformed magic number of neutrons

($N = 62$) of quadrupole deformed fragment. However, the asymmetric fission involving octupole deformed fragment ($Z = 56$; ^{144}Ba or in its vicinity) is found prominent in the case of heavier isotopes of Th, i.e. $^{226,228,230}\text{Th}^*$. From above analysis, the near-symmetric and asymmetric fission modes observed in the decay of Th isotopes, due to involvement of deformations (up to β_3) and related cold optimum orientation, are in agreement with the experimental results.

Such investigations help in understanding the fission dynamics especially in the asymmetric region of heavy-mass actinides. For further studies, one can explore the relevance and importance of octupole deformed fragments decaying from heavy and superheavy nuclei.

V. ACKNOWLEDGMENT

The financial support from Council of Scientific & Industrial Research (CSIR), in the form of a Senior Research Fellowship, DAE, Government of India, sanction no. 58/14/12/2019-BRNS and UGC-DAE consortium for Scientific Research, File No. UGC-DAE-CSR-KC/CRS/19/NP09/0920 are gratefully acknowledged.

-
- [1] S. Hoafmann and G. Munzenberg, *Rev. Mod. Phys.* **72**, 733 (2000).
- [2] S. Hofmann *et al*, *Eur. Phys. J. A* **14**, 147 (2002).
- [3] Y. T. Oganessian *et al*, *Phys. Rev. C* **70**, 064609 (2004).
- [4] Y. T. Oganessian, *J. Phys. G* **34**, R165 (2007).
- [5] U. Brosa, S. Grossmann and A Muller, *Phys. Rep.* **197**, 167 (1990).
- [6] K. Nisho *et al*, *Phys. Rev. C* **77**, 064607 (2008).
- [7] R. K. Gupta *et al*, *J. Phys. G: Nucl. Part. Phys.* **31**, 631-644 (2005).
- [8] A. Sandulescu *et al*, *Phys. Lett. B* **60**, 225 (1976).
- [9] R. K. Gupta, A. Sandulescu and W. Greiner, *Phys. Lett. B* **67**, 257 (1977).
- [10] R. K. Gupta, C. Parvulescu, A. Sandulescu and W. Greiner, *Z. Phys. A* **283**, 217 (1977).
- [11] R. K. Gupta, A. Sandulescu and W. Greiner, *Z. Naturforsch.* **32a**, 704 (1977).
- [12] A. Sandulescu, D. N. Poenaru and W. Greiner, *Sov. J. Nucl.* **11**, 528 (1980).
- [13] D. N. Poenaru *et al*, *J. Phys. G: Nucl. Phys.* **10**, L183-L189 (1984).
- [14] D. N. Poenaru, W. Greiner, M. Ivascu and A. Sandulescu, *Phys. Rev. C* **32**, 6 (1985).
- [15] D. N. Poenaru and W. Greiner, *J. Phys. G: Nucl. Phys.* **17**, S443-S451 (1991).
- [16] K.-H. Schmidt *et al*, *Nucl. Phys. A* **665**, 221-267 (2000).
- [17] D. N. Poenaru, Y. Nagame, R. A. Gherghescu and W. Greiner, *Phys. Rev. C* **65**, 054308 (2002).
- [18] D. N. Poenaru, R. A. Gherghescu and W. Greiner, *Phys. Rev. C* **83**, 014601 (2011).
- [19] M. Kaur, M. K. Sharma and R. K. Gupta, *Phys. Rev. C* **86**, 064610 (2012).
- [20] K.-H. Schmidt and B. Jurado, *Rep. Prog. Phys.* **81**, 106301 (2018).
- [21] A. N. Andreyev, K. Nishio and K.-H. Schmidt, *Rep. Prog. Phys.* **81**, 016301 (2018).
- [22] A. Kaur, N. Sharma and M. K. Sharma, *Phys. Rev. C* **103**, 034618 (2021).
- [23] L. P. Gaffney *et al*, *Nature* **497**, 199-204 (2013).
- [24] B. Bucher *et al*, *Phys. Rev. Lett.* **116**, 112503 (2016).
- [25] S. Jain, M. K. Sharma and R. Kumar, *Phys. Rev. C* **101**, 051601(R) (2020).
- [26] S. Jain, M. K. Sharma and R. Kumar, *Chinese Physics C* (Accepted), DOI: <http://doi.org/10.1088/1674-1137/ac2ed2>.
- [27] G. Scamps and C. Simenel, *Nature* **564**, 382 (2018).
- [28] R. K. Gupta, in *Clusters in Nuclei*, Lectures Notes in Physics **818**, Vol. I, edited by C. Beck (Springer-Verlag, Berlin, 2010), p.223.
- [29] D. Jain, R. Kumar and M. K. Sharma, *Phys. Rev. C* **87**, 044612 (2013).
- [30] A. Kaur and M. K. Sharma, *Nucl. Phys. A* **99**, 044611 (2019).
- [31] H. J. Fink, J. Maruhn, W. Scheid, and W. Greiner, *Z. Phys.* **268**, 321 (1974).
- [32] J. Maruhn and W. Greiner, *Phys. Rev. Lett.* **32**, 548 (1974).
- [33] R. K. Gupta, W. Scheid, and W. Greiner, *Phys. Rev. Lett.* **35**, 353 (1975).
- [34] M. Dasgupta *et al*, *Phys. Rev. Lett.* **99**, 192701 (2007).
- [35] R. K. Gupta and W. Greiner, “*Heavy elements and related new phenomena*”, edited by W. Greiner and R. K. Gupta, Vol. I, p. 536 (World Scientific, Singapore, 1999).
- [36] J. Maruhn and W. Greiner, *Phys. Rev. L* **32**, 10 (1974).
- [37] R. K. Gupta, W. Scheid and W. Greiner, *Phys. Rev. L* **35**, 6 (1975).

- [38] H. Kroger and W. Scheid, J. Phys. G **6**, L85 (1980).
- [39] R. Dutt, A. Khare and U. P. Sukhatme, American Journal of Physics **59**, 723 (1991).
- [40] H. S. Khosla and S. S. Malik, Nucl. Phys. **A513**, 115-124 (1990).
- [41] S. Kumar and R. K. Gupta, Phys. Rev. C **55**, 1 (1997).
- [42] R. K. Gupta, S. Kumar and W. Scheid, Int. J Mod. Phys. E, Vol. **6**, No. 2, 259-274 (1997).
- [43] S. J. Sanders *et al*, Phys. Rev. C **40**, 2091 (1989).
- [44] S. Sander, Phys. Rev. C **44**, 2676 (1991).
- [45] T. Matsuse, Phys. Rev. C **55**, 1380 (1997).
- [46] N. J. Davidson *et al*, Nucl. Phys. A **570**, 61c (1994).
- [47] P. A. Seeger, Nucl. Phys. **25**, 1 (1961).
- [48] S. DeBenedetti, Nuclear Interactions (New York: book Published by Wiley Sons) (1964).
- [49] W. Myers and W. J. Swiatecki, Nucl. Phys. **81**, 1 (1966).
- [50] C. Y. Wong, Phys. Rev. Lett. **31**, 766 (1973).
- [51] P. MÅoller, J. R. Nix, W. D. Myers, and W. J. Swiatecki, At. Data Nucl. Data Tables **59**, 185 (1995).
- [52] A. Bohr, Mat. Fys. Medd. Dan. Vid. Selsk, Vol. **26**, No. 14 (1952).
- [53] A. Bohr and B. R. Mottelson, Mat. Fys. Medd. Dan. Vid. Selsk, Vol. **27**, No. 16 (1953).
- [54] S. Shlomo and J. B. Natowitz, Phys. Rev. C **44**, 2878 (1991).
- [55] J. Blocki *et al*, Ann. Phys. (NY) **105**, 427 (1977).
- [56] K. J. LeCouteur and D. W. Lang, Nucl. Phys. **13**, 32 (1959).
- [57] M. Seiwert *et al*, Phys. Rev. C **29**, 477 (1984).
- [58] N. Malhotra and R. K. Gupta, Phys. Rev. C **31**, 1179 (1985).
- [59] R. K. Gupta, N. Singh, and M. Manhas, Phys. Rev. C **70**, 034608 (2004).
- [60] M. Manhas and R. K. Gupta, Phys. Rev. C **72**, 024606 (2005).
- [61] M. K. Sharma, G. Sawhney, R. K. Gupta and W. Greiner, J. Phys. G: Nucl. Part. Phys. **38**, 105101 (2011).
- [62] N. Gover, I. Sharma, G. Kaur and M. K. Sharma, Nucl. Phys. A **959**, 10-26 (2017).
- [63] B. Bucher *et al*, Phys. Rev. Lett. **118**, 152504 (2017).
- [64] A. Chatillo *et al*, Phys. Rev. C **99**, 054628 (2019).
- [65] H. Pasca *et al*, Phys. Rev. C **94**, 064614 (2016).